Biosensors and Bioelectronics 35 (2012) 349–354

Contents lists available at SciVerse ScienceDirect

Biosensors and Bioelectronics

journal homepage: www.elsevier.com/locate/bios

Fabrication of stratified nanoporous gold for enhanced biosensing

Huajun Qiu*, Feixue Zou

School of Chemistry and Chemical Engineering, Shandong University, Jinan 250100, China

ARTICLE INFO

Article history:
Received 27 January 2012
Received in revised form 8 March 2012
Accepted 9 March 2012
Available online 18 March 2012

Keywords:
Hierarchical
Dealloying
Enzyme immobilization

ABSTRACT

By a dealloying/annealing/redealloying strategy, nanoporous gold (NPG) with hierarchical microstructure is fabricated for electrochemical biosensing application. The first dealloying and annealing would produce NPG/AuAg alloy composite with a large-pore NPG layer and the second dealloying would further etch the AuAg alloy part in the composite, generating a small-pore NPG layer. By using the large-pore (~100 nm) layer as the glucose oxidase (GOx) container, and the small-pore (~12 nm) layer as a signal producer, this novel hierarchical NPG is demonstrated to be a good support for enzyme immobilization and fabricating enzyme-based biosensors. The immobilized GOx retains ~92% of the initial activity after 7 repeated use. The GOx-loaded stratified NPG biosensor can detect glucose more sensitively with a wider linear range (up to 22 mM) than normal NPG with a uniform pore size of 30–40 nm (linear range: up to 17 mM).

1. Introduction

Nanoporous metals have been attracting much interest in the fields of catalysis, fuel cells, sensors, actuator, surface-enhanced Raman scattering, etc. (Ciesielski et al., 2008; Ding et al., 2004a; Hu et al., 2008; Huang and Sun, 2004; Jia et al., 2007a,b; Kafi et al., 2010; Lee and Park, 2010; Liu et al., 2009; Liu and Searson, 2006; Scanlon et al., 2012; Shin et al., 2008; Wang et al., 2008; Xia et al., 2011; Yu et al., 2006; Zhang et al., 2009a,b; Zielasek et al., 2006) Among various nanoporous metals, nanoporous gold (NPG) prepared by dealloying AuAg alloy is of special interest due to not only its unique physicochemical properties but also its biocompatibility (Biener et al., 2006; Ding et al., 2004b; Dong and Cao, 2008; Erlebacher et al., 2001; Wittstock et al., 2010; Zielasek et al., 2006). For example, NPG exhibits remarkable catalytic activities for low-temperature oxidation of CO (Xu et al., 2006; Zielasek et al., 2006) and selective oxidation of alcohols (Wittstock et al., 2010). Besides its inherent catalytic activity, NPG has also been demonstrated to be a good three-dimensional (3D) support for other catalysts such as enzymes, nanostructured Pt, etc., due to the tunable pore size, good biocompatibility, and excellent electron conductivity (Ding et al., 2004a; Ge et al., 2009; Qiu et al., 2008, 2009a; Shulga et al., 2007). The fabricated composite materials further extend the application fields of NPG. For example, Pt/NPG can be used in fuel cells and generate a specific power of 1.75 kW g^{-1} Pt, which is larger than the value of commercially available membrane electrode assembly (~1.0 kW g^{-1} Pt) (Ding et al., 2004a). Alcohol dehydrogenase and glucose oxidase (GOx) loaded NPG can sensitively detect ethanol and glucose, respectively (Qiu et al., 2009b).

It is well-known that the physicochemical properties of nanomaterials are related with their microstructures. Fabrication of nanomaterials with controllable structure is very important for studying the structure-related properties and their potential applications. For NPG obtained by dealloying, it has been demonstrated that its microstructure (pore/ligament size) can be tailored by changing alloy compositions, dealloying conditions, and annealing conditions after the dealloying (Ding et al., 2004b; Qian and Chen, 2007). For example, the pore size of NPG obtained by dealloying AuAg alloy (50 wt.%, Au) increases from ~8 nm to ~40 nm when extending the dealloying time from 5 min to 1 day (Ding et al., 2004b). The pore size of NPG can be further increased to several hundred nanometers by annealing at high temperatures (over 100 °C) (Ding et al., 2004b). Although the pore/ligament size can be tailored by adjusting these experimental parameters, a systematic study on how these experimental parameters affect the microstructure evolution is still lacking. On the other hand, NPG prepared by simply changing these parameters has a homogeneous microstructure.

For specific applications, however, the fabrication of nanoporous metals with hierarchical microstructure is more desirable. For example, in microfluidic-based sensors, larger pores (100 s of nm) are useful in microfluidic flow control, whereas the small pores (10 s of nm) are useful for increasing device surface area and sensitivity. For some enzyme-based biosensors, the large pores facilitate the loading of biomacromolecules (enzymes) and the small pores with a high surface area facilitate the mass transfer of small molecules and their sensitive detection. However, the fabrication of hierarchical NPG with multimodal pore/ligament structure by the dealloying strategy has been rarely

* Corresponding author.
E-mail address: qiuhuajun@gmail.com (H. Qiu).

0956-5663/$ – see front matter © 2012 Elsevier B.V. All rights reserved.
doi:10.1016/j.bios.2012.03.015

reported. Ding and Erlebacher (2003) reported a dealloying/Ag plating/redealloying strategy to create NPG with bimodal pore size distributions. In their work, NPG was used as the template for Ag plating, and then annealing was applied to homogenize Ag with Au and enlarge the pore size. The second dealloying then generated the secondary pores.

In this work, using AuAg alloy as the precursor alloy, we first systematically study the microstructure evolution of NPG under different dealloying and annealing conditions. Then by the combination of controlled dealloying and annealing, NPG with stratified microstructure is successfully fabricated for the fabrication of enzyme-based biosensors. As far as we know, this is the first report on the fabrication of this novel stratified NPG. Moreover, this stratified NPG is demonstrated to be a good support for GOx and fabrication of sensitive oxidase-based electrochemical biosensor.

2. Experimental

2.1. Reagents

GOx and Nafion were purchased from Sigma–Aldrich. Horseradish peroxidase (HRP), ascorbic acid, acetamidophenol, uric acid, H_2O_2 and glucose were purchased from Sinopharm Chemical Reagent Ltd. Co. Other chemicals were of analytical grade. Triply distilled water and PBS (50 mM, pH 7.0) were used throughout the experiments.

2.2. Apparatus

The microstructure of NPG was characterized with a JEOL JSM-6700F field emission scanning electron microscope (SEM) equipped with an Oxford INCA x-sight energy dispersive X-ray spectrometer (EDS). The absorbance data was recorded on a Shimadzu UV-2550 spectrophotometer. Electrochemical experiments were performed on a CHI 660C electrochemical work station. A three-electrode system was used, including a NPG-based working electrode, platinum gauze counter electrode and saturated calomel electrode (SCE) reference electrode.

2.3. Preparation of NPG

$Au_{30}Ag_{70}$ alloy (at.%) was made by melting high purity (>99.9%) Au and Ag at a high temperature, followed by cold-rolling. The $Au_{30}Ag_{70}$ alloy foils with a thickness of 25 μm were used for the study of NPG structure evolution under different experimental conditions. The alloy foils with a thickness of 50 μm were used for the preparation of stratified NPG. Nitric acid (~65%) was used as the dealloying solution throughout the experiments. Annealing of NPG was carried out in a furnace with controllable heating device. Before the annealing treatment, NPG was carefully washed with pure water. For comparison study of the biosensing performance, normal NPG with a uniform pore/ligament size of 30–40 nm was also prepared by dealloying the $Au_{30}Ag_{70}$ (50 μm in thickness) in HNO_3 solution (~65%) for 1000 min at 25 °C.

2.4. GOx immobilization and activity test

GOx was immobilized on a two-layer NPG (size: 3 mm × 3 mm × 50 μm) by dropping 4 μL GOx stock solution (5 mg mL^{-1}) on the surface of the large-pore layer. After dried at 4 °C, the surface of the large-pore layer was sealed by coating with adhesive. At room temperature (25 °C), under mild stirring, the GOx/NPG was added into 3 mL of buffer solution (PBS, pH 7.0) containing 5 mM glucose, 0.3 mM O-phenylenediamine (OPD) and 0.01 mg HRP to initiate the enzyme-catalyzed reaction. A plot of absorbance at 448 nm vs. time was recorded on a Shimadzu UV-2550 spectrophotometer. The molar extinction coefficient of the oxidation product of OPD at 448 nm was 10.6 mM^{-1} cm^{-1}. For repeated use, the GOx/NPG biocomposite was taken out from the reaction mixture after 5 min reaction and rinsed three times with the PBS. Then the biocomposite was added into the same but fresh reaction solution for the next use.

2.5. Leaching test

The GOx/NPG was mixed with 1 mL PBS (pH 7.0, 50 mM) under mild stirring for 1 h, and then the GOx/NPG was removed. The remainder solution was tested using the Bradford method.

2.6. Biosensor fabrication and biosensing

The stratified NPG-based biosensor was made by connecting the large-pore side sealed GOx/stratified NPG with a gold wire because NPG is a macroscopic nanomaterial. Normal NPG-based biosensor was made by a similar way except that the unsealed side was covered with a Nafion (2 μL, 0.05 wt.%) film to avoid GOx leakage. The current response of the biosensor to each addition of glucose was recorded at −0.2 V vs. SCE.

3. Results and discussion

NPG has been demonstrated to be a good support for biomacromolecules (such as enzymes) and the fabrication of electrochemical bio-nanodevice due to its large surface area, controllable pore size, good electron conductivity and biocompatibility (Qiu et al., 2008). In this work, we aim to fabricate a new kind of hierarchical NPG with different pore size distributions for enhanced enzyme-based biosensing. The big-pore part is used as a container for enzyme and the small-pore part with a high surface area is used as a detector for the enzymatic product with fast response and high sensitivity. Before fabricating the hierarchical NPG using bulk AuAg alloy, we first examined the microstructure evolution of AuAg alloy under different dealloying conditions.

3.1. Effects of dealloying time and temperature

At room temperature (25 °C), the etched thickness of the alloy at different etching time is first studied by monitoring the cross-sectional change of the alloy with SEM. As shown in Fig. 1a, after 2 min dealloying, the etching can reach to ~1 μm depth. The alloy foil is penetrated through after ~16 min dealloying, forming a 3D bicontinuous nanoporous structure. The change of Ag content with increasing etching time is also recorded (Fig. 1b). When the alloy foil is penetrated through at 16 min, ~50 at.% of Ag is remained. The dealloying rate of Ag is 1.25 at.% min^{-1} during the first 16 min. From 16 to 64 min, the Ag content is dealloyed to be ~12 at.% with the dealloying rate of 0.79 at.% min^{-1} in this period. When the dealloying time is over 64 min, the Ag content drops to less than 10 at.% and then the Ag content changes very slowly with the dealloying time. At 16 min (the penetration through and formation of complete nanoporous structure), the surface area of the sample reaches the highest value. Thus, the decreased dealloying rate should be caused by the passivation effect of gold at the alloy/electrolyte interface. It can be concluded that the dealloying rate of Ag decreases with increasing etching time. For the pore size evolution with the dealloying time, it is observed that from 0 to 16 min, the pore size of NPG increases dramatically from 0 to ~16 nm (inset in Fig. 1c). After the penetration of the alloy at 16 min, the coarsening of pores becomes slow (Fig. 1c). This result indicates that the slower dealloying rate of Ag would result in a slower pore/ligament coarsening. This slowdown of pore/ligament coarsening with the increase of etching time

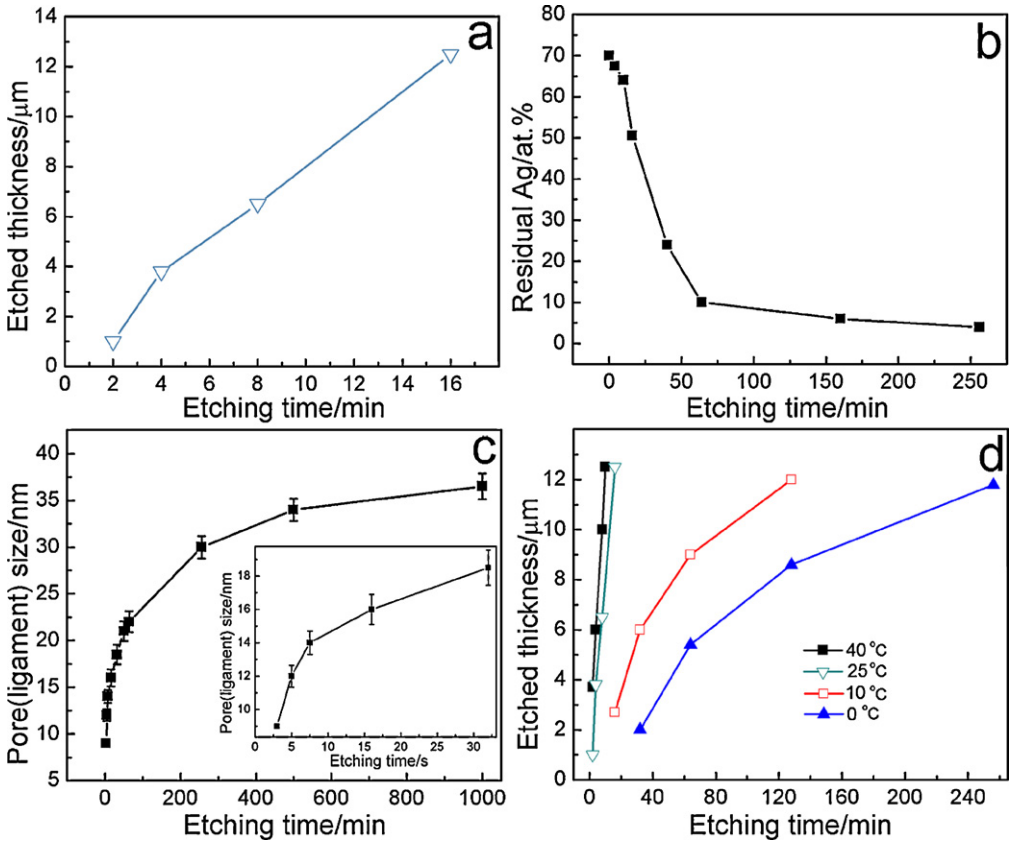

Fig. 1. Etched thickness of the alloy with etching time at 25 °C (a); changes of Ag content (b) and the pore (ligament) size (c) of NPG with etching time at 25 °C, inset in (c) is the enlarged image from 0 to 32 min; etched thickness of the alloy with etching time at different temperatures (d).

also explains why the pore sizes of NPG (both surface and inner) are usually quite uniform although the surface sites are dealloyed for a longer time compared with inner sites.

To explain the formation mechanism of the nanoporous structure during dealloying, an atomistic model was proposed by Erlebacher et al. (Erlebacher et al., 2001) This model involves a kind of "interfacial phase separation" in which Ag atoms are dissolved and the left gold atoms from the alloy/electrolyte interface would self-organize and form a 3D bicontinuous network of pores and ligaments. Due to the fast surface diffusion of Au in the solid/electrolyte surface, even when the Ag content changes negligibly after 256 min (Fig. 1b), the pore size of NPG continues to increase slowly when NPG is in contact with the dealloying solution (Fig. 1c). The coarsening can be stopped by simply removing NPG from the etching solution to water.

The dealloying of $Au_{30}Ag_{70}$ is further studied under different temperatures. As shown in Fig. 1d, at a low etching temperature (0 °C), the dealloying rate (the penetration of the AuAg alloy) becomes much slower. Only 2 μm of thickness is penetrated after 32 min. For the complete penetration through, 256 min is needed. With the increase of etching temperature, the penetration through of the AuAg alloy becomes much faster. For example, at 40 °C only 12 min is needed for the penetration through. The etching temperature also has a significant effect on the length scale of NPG microstructure. With the same dealloying time (64 min), the pore/ligament sizes increase from ~10 nm at 0 °C to ~30 nm at 40 °C (Fig. S-1 in Supporting information (SI)). Based on the surface diffusion controlled coarsening mechanism, the diffusivity (D_s) of Au atoms at each etching temperature can be estimated by the equation (Qian and Chen, 2007): $D_s = d(t)^4 kT/32\gamma t\alpha^4$ where $d(t)$ is pore size at etching time t, k is Boltzmann constant, T is the etching temperature, γ is surface energy, and α is the lattice parameter. According to the data obtained in this work and the parameters compiled in Ref. (Dursun et al., 2003), the surface diffusivity of Au in HNO_3 at 0 °C and 40 °C are estimated to be 1.1×10^{-20} and 1.0×10^{-18} $m^2\,s^{-1}$, respectively. Therefore, the small temperature change from 0 °C and 40 °C can increase the diffusivity of Au by nearly two orders of magnitude, resulting in a coarsened microstructure. The strong temperature dependence of pore/ligament size observed in this work is in good agreement with kinetic Monte Carlo simulation where low diffusivity (D_s) of Au atoms leads to a small pore/ligament size (d) (Erlebacher et al., 2001).

3.2. Effects annealing

It is noted from both the present work and literatures that it is hard to prepare NPG with a pore/ligament size over 100 nm by simply extending the dealloying time at room temperature (Ding et al., 2004b). The pore/ligament size of NPG can be further enlarged by an annealing step after the dealloying. As shown in Fig. S-2a (SI), after 1 h annealing of NPG with a pore/ligament size of ~25 nm at 200 °C, the pore/ligament size increases to ~100 nm. One-hour annealing at 300, 400 and 500 °C would enlarge the pore/ligament size of the NPG to about 150, 400 and 500 nm, respectively. The high temperature would induce the fast mobilization of surface Au atoms, resulting in coarsened microstructure. The microstructure coarsening of NPG with increasing annealing time at a fixed temperature (400 °C) has also been studied. The pore/ligament sizes of NPG increase almost linearly with the increase of annealing time at 400 °C (Fig. S-2b in SI), indicating that the pore/ligament sizes can also be adjusted by changing the annealing time.

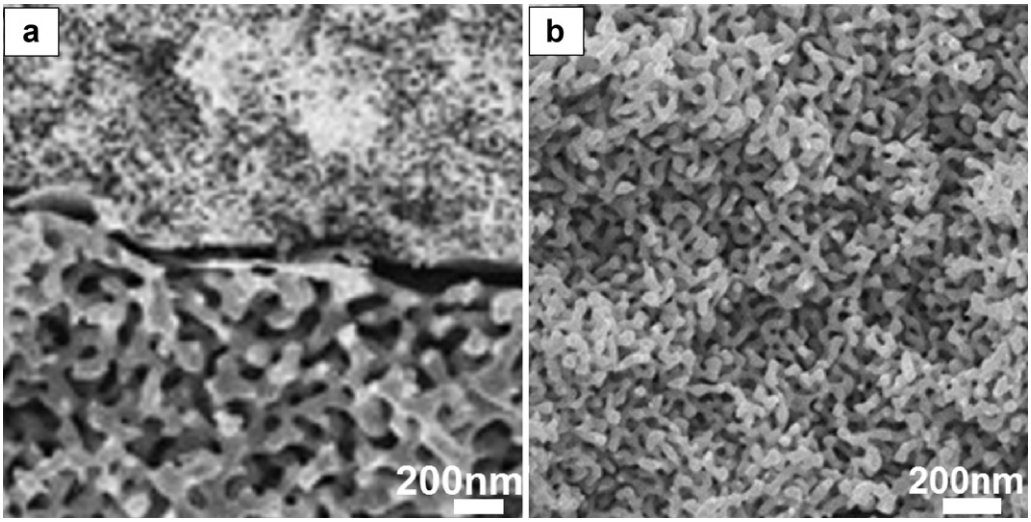

Fig. 2. Cross-sectional SEM images of a two-layer NPG obtained by 30 min initial dealloying at 30 °C, 1 h annealing at 200 °C and 10 h redealloying at 0 °C (a), and normal NPG obtained by 1000 min dealloying at 25 °C (b).

3.3. Fabrication of stratified NPG for biosensing

Based on the microstructure evolution of NPG under different experimental conditions, in this section, by reasonably controlling these experimental parameters, we fabricated a two-layer NPG with similar layer thickness for enzyme-based electrochemical biosensing application. For a typical preparation of the two-layer NPG, we applied a dealloying/annealing/redealloying strategy. Specifically, the precursor alloy with one side protected was first etched for a certain time (less than the penetration time), and then the unpenetrated NPG (i.e., NPG/AuAg alloy composite) was annealed at a high temperature to enlarge the pore size in the NPG part. The NPG/AuAg alloy composite was then re-dealloyed to completely penetrate the AuAg alloy and generate the small-pore part (layer). As shown in Fig. 2a, this approach can create a well-defined two-layer NPG with different pore size distributions. It is worth mentioning that without the one-side protection, this strategy can fabricate three-layer NPG with symmetric microstructure. It is also expected that if we use a thicker AuAg alloy and repeat the dealloying/annealing/redealloying process, NPG with multiple layers can also be fabricated.

For the enzyme-based biosensing application, it has been reported that nanoporous structure with a large pore size of ~100 nm can facilitate both enzyme loading and their catalytic reaction (Qiu et al., 2010), while nanoporous structure with a small pore size and large surface area is more sensitive for small molecule detection. Thus, with a similar layer thickness, the pore size of the large-pore layer is adjusted to ~100 nm and the pore size of the small-pore layer is adjusted to ~12 nm (Fig. 2a) to make the two-layer NPG suitable for enzyme-based biosensor fabrication. Note that further decreasing the small pore size to less than 10 nm under the free dealloying condition is hard to achieve due to the fast diffusivity of Au atoms at solid/electrolyte interface. The fabrication condition for this two-layer NPG is initial dealloying for 30 min at 30 °C, annealing at 200 °C for 1 h and redealloying at 0 °C for 10 h. GOx is immobilized by simply dropping 4 μL GOx stock solution (5 mg mL^{-1}) on the large-pore NPG layer and drying it at 4 °C. Then the surface of the large-pore side is sealed with adhesive and the whole piece of NPG is connected with a gold wire.

Before testing the electrochemical biosensing performance for glucose, the enzymatic properties (enzyme activity and stability) of the immobilized GOx and the electrocatalytic activity of the stratified NPG are first studied. GOx can catalyze the oxidation of glucose by oxygen producing H_2O_2 which can be used as oxidant for the oxidation of OPD catalyzed by HRP. The oxidation product of OPD would give absorption of light at 448 nm (Qiu et al., 2010). Thus, the catalytic activity of GOx can be correlated with the absorption change at 448 nm. As expected, the immobilized GOx shows high catalytic activity and stability. Compared with free GOx, the specific activity of the immobilized one retains more than 80%. This value is larger than that of laccase immobilized on NPG with a uniform pore size of 40–50 nm by physical adsorption (75% laccase activity is retained) (Qiu et al., 2009a), which should be due to the larger pore size in this work and the embedding strategy for GOx immobilization. In this way, more GOx would have less contact with the gold surface, which would facilitate the enzyme to function. As shown in Fig. S-3 (SI), the immobilized GOx also exhibits excellent reusability. After 7 repeated use, the catalytic activity of the immobilized GOx still retains ~92% of its initial activity, indicating the leaching out of GOx should be negligible. For further demonstration, the GOx/stratified NPG is immersed in the PBS leaching solution (pH 7.0, 50 mM) for 1 h under a mild stirring condition. After the removal of the GOx/stratified NPG, no GOx is detected in the PBS solution by the Bradford method. The good stability of the GOx/stratified NPG can be explained as follows. Since the surface of the large-pore layer is sealed, the transportation of small molecules (enzymatic substrates and products) would be through the small-pore layer. The small-pore layer allows the free transportation of small molecules but blocks the leaching of the biomacromolecules (GOx). In fact, this result is in good agreement with our previous observation that when the pore size of NPG is between 10 and 20 nm, laccase (~8 nm in diameter) cannot get inside of the microstructure (Qiu et al., 2008). Besides the immobilization strategy, the activity of GOx is also greatly influenced by the solution pH and temperature. In this work, it is observed that both the free and immobilized GOx exhibit similar activity-pH profiles from pH 3.5 to 7.5 with the optimum pH at 5.5 (Fig. S-4 in SI). At a fixed pH of 5.5, the initial activities of both GOx increase with the increase of temperature (20–60 °C). However, for the purpose of glucose biosensing, a pH value of 7.0 and room temperature are selected because the pH of plasma glucose is around 7.0 and the stability of GOx decreases dramatically with increasing reaction temperature (although the initial activity of GOx is higher at a higher temperature). This glucose detection condition, i.e., neutral pH and room temperature, is frequently used for GOx-based biosensors.

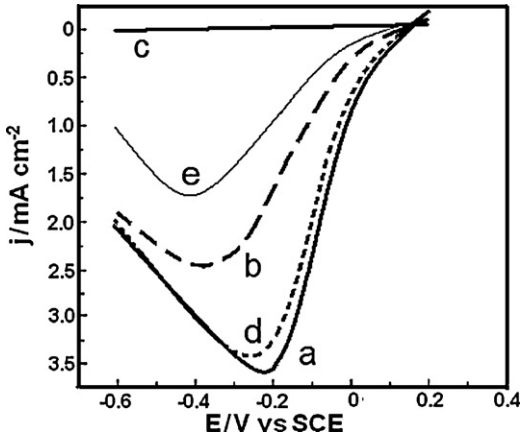

Fig. 3. Linear sweep voltammetry curves of a bare stratified NPG (a and c) with pore sizes of 12 nm and 100 nm on each layer and normal NPG with a uniform pore/ligament size of 30–40 nm (b) in PBS (50 mM, pH 7.0) with (a and b) and without (c) 5 mM H_2O_2; linear sweep voltammetry curves of GOx/stratified NPG (d) and GOx/normal NPG (e) in PBS (50 mM, pH 7.0) containing 5 mM H_2O_2.

The electrocatalytic activity of the stratified NPG toward H_2O_2 reduction is shown in Fig. 3. For comparison, normal NPG with a uniform pore size of 30–40 nm (its SEM image is shown in Fig. 2b) is also tested. As observed, the stratified NPG with a fine pore/ligament size of ~12 nm on the surface shows remarkably improved current response for H_2O_2 reduction compared with the normal NPG. Moreover, the peak potential is negatively shifted by ~90 mV, indicating the faster reaction kinetics on the stratified NPG surface. Because NPG with a smaller ligament size contains more Ag atoms, the small-pore layer of the stratified NPG should be nanoporous AuAg alloy. For NPG with a uniform pore/ligament size of 30–40 nm, the Ag content is less than 5 at.%. Therefore, the alloy effect might explain the improved electrocatalytic activity of the fine ligaments. It has been demonstrated that the residual Ag in NPG plays an important role for its high catalytic activity toward CO oxidation (Wittstock et al., 2009). In addition, it has been widely accepted that metal nanocatalyst with a smaller particle size usually has a higher catalytic activity due to the more strained surface. The electrocatalytic activities of the two GOx-loaded NPG toward H_2O_2 reduction are also tested. As shown in Fig. 3d and e, after GOx immobilization, the current response on the stratified NPG only slightly decreases, while the current response on the normal NPG decreases to ~70% of the initial value. The remarkable current decrease on the GOx/normal NPG should be due to the reduction of the active surface area by GOx adsorption on gold ligaments. For the GOx/stratified NPG, GOx are trapped in the big-pore layer. Thus, the active surface area which mainly comes from the small-pore layer is well-preserved. This result strongly indicates that the stratified NPG should be a better electrode material for enzyme-based electrochemical biosensor fabrication compared with normal NPG.

The performance of the stratified NPG-based biosensor is then tested by recording its amperometric response to the added glucose under −0.2 V (vs. SCE). It is worth mentioning that at this low potential the current from the direct oxidation of glucose on NPG is negligible. Fig. 4a shows the amperometic response of the GOx/stratified NPG toward each addition of 1.0 mM glucose. As observed, this novel biosensor responses sensitively to each addition of glucose. The signal reaches the highest value within 4 s, indicating that glucose can diffuse freely into the nanoporous structure and be quickly oxidized by GOx-catalyzed reaction. As shown in Fig. 4b, it exhibits a wide linear range from 0 to 22 mM (R = 0.996) for glucose sensing with a detection limit of ~10 μM (S/N = 3). In comparison, the GOx/normal NPG has a much lower current response and shorter linear range (0–17 mM). The linear range of the GOx/stratified NPG biosensor is also wider than other biosensors such as GOx/CNT/nano-Pt (25 nM to 2 mM) (Male et al., 2007), GOx/porous PtNi (0.5–21 mM) (Qiu et al., 2012), GOx/CNT/Teflon (2–20 mM) (Wang and Musameh, 2003) and GOx/graphene (0.01–10 mM) (Zhou et al., 2009) biosensors. The enhanced performance of the GOx/stratified NPG biosensor is clearly due to the high activity of imbedded GOx and the existence of the small-pore layer which has a higher electrocatalytic activity and larger active surface area. For the interference test, the physiological level of ascorbic acid (0.1 mM), acetamidophenol (0.1 mM) and uric acid (0.02 mM) show no obvious response at the GOx/stratified NPG biosensor due to the low detection potential (Fig. 5a). Moreover, the GOx/stratified NPG biosensor also exhibits enhanced durability. After continuous working for 1500 s, the current response on the GOx/stratified NPG changes negligibly, while that on the GOx/normal NPG decreases to ~90% of its initial value (Fig. 5b). All these suggest that the GOx/stratified NPG biosensor should satisfy the need for the fast, sensitive and stable detection of plasma glucose (3–8 mM). In addition, the stratified NPG-based biosensor is also reproducible and stable. For 5 mM glucose, the relative standard deviation (RSD) of five freshly prepared NPG biosensors is ~4.6%. After 1 month storage at 4 °C, the response of the biosensor remains ~96% of its initial value. The excellent performance of this stratified NPG-based biosensor suggests the promising future of the stratified NPG for the fabrication of other electrochemical bio-nanodevices.

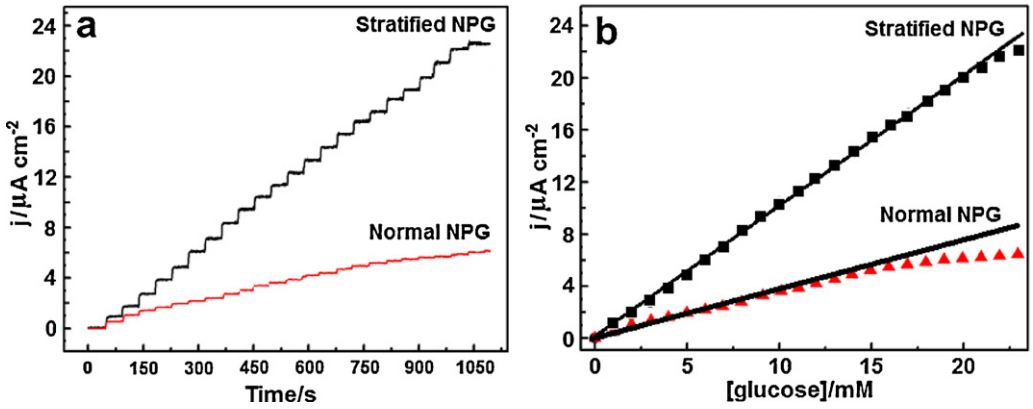

Fig. 4. Amperometric responses of GOx/stratified NPG and GOx/normal NPG on successive addition of 1.0 mM glucose into the stirring PBS (50 mM, pH 7.0), applied potential: −0.2 V (a); plots of currents vs. glucose concentrations (b).

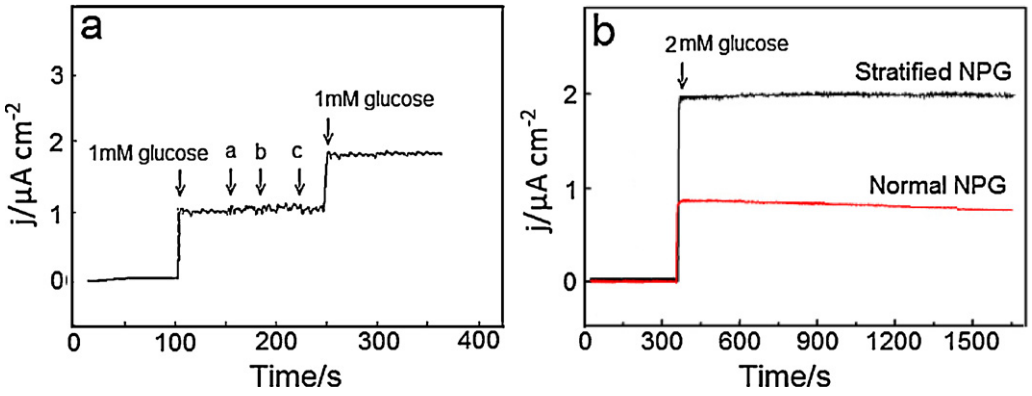

Fig. 5. Amperometric responses of GOx/stratified NPG on successive addition of glucose and different interfering species (a: 0.1 mM ascorbic acid, b: 0.1 mM acetamidophenol and c: 0.02 mM uric acid) into the stirring PBS (50 mM, pH 7.0) (a); long-term amperometric responses of GOx/stratified NPG and GOx/normal NPG on addition of 2.0 mM glucose into the stirring PBS (50 mM, pH 7.0) (b). Applied potential: −0.2 V.

4. Conclusions

By a dealloying/annealing/redealloying strategy, stratified NPG with different pore size distributions is fabricated. With the large-pore layer as the enzyme container and the small-pore layer as the detector for the enzymatic product, this novel stratified NPG is demonstrated to be a good support for the fabrication of enzyme-based biosensors. In a poof-of-concept study, the GOx-loaded two-layer NPG with pore sizes of ~100 nm and ~12 nm in each layer can more sensitively detect glucose with a wider linear range compared with GOx-loaded normal NPG with a uniform pore size of 30–40 nm. This kind of macroscopic nanomaterial with controllable hierarchical porosity should be promising in the fields of sensors, actuators, micro-reactors, etc.

Acknowledgment

This work was supported by Shandong University.

Appendix A. Supplementary data

Supplementary data associated with this article can be found, in the online version, at doi:10.1016/j.bios.2012.03.015.

References

Biener, J., Hodge, A.M., Hayes, J.R., Volkert, C.A., Zepeda-Ruiz, L.A., Hamza, A.V., Abraham, F.F., 2006. Nano Lett. 6, 2379–2382.
Ciesielski, P.N., Scott, A.M., Faulkner, C.J., Berron, B.J., Cliffel, D.E., Jennings, G.K., 2008. ACS Nano 2, 2465–2472.
Ding, Y., Chen, M.W., Erlebacher, J., 2004a. J. Am. Chem. Soc. 126, 6876–6877.
Ding, Y., Erlebacher, J., 2003. J. Am. Chem. Soc. 125, 7772–7773.
Ding, Y., Kim, Y.J., Erlebacher, J., 2004b. Adv. Mater. 16, 1897–1900.
Dong, H., Cao, X., 2008. J. Phys. Chem. C 113, 603–609.
Dursun, A., Pugh, D.V., Corcoran, S.G., 2003. J. Electrochem. Soc. 150, B355–B360.
Erlebacher, J., Aziz, M.J., Karma, A., Dimitrov, N., Sieradzki, K., 2001. Nature 410, 450–453.
Ge, X., Yan, X., Wang, R., Tian, F., Ding, Y., 2009. J. Phys. Chem. C 113, 7379–7384.
Hu, K., Lan, D., Li, X., Zhang, S., 2008. Anal. Chem. 80, 9124–9130.
Huang, J.-F., Sun, I.W., 2004. Chem. Mater. 16, 1829–1831.
Jia, F., Yu, C., Ai, Z., Zhang, L., 2007a. Chem. Mater. 19, 3648–3653.
Jia, F., Yu, C., Deng, K., Zhang, L., 2007b. J. Phys. Chem. C 111, 8424–8431.
Kafi, A.K.M., Ahmadalinezhad, A., Wang, J., Thomas, D.F., Chen, A., 2010. Biosens. Bioelectron. 25, 2458–2463.
Lee, Y.-J., Park, J.-Y., 2010. Biosens. Bioelectron. 26, 1353–1358.
Liu, L.F., Pippel, E., Scholz, R., Gosele, U., 2009. Nano Lett. 9, 4352–4358.
Liu, Z., Searson, P.C., 2006. J. Phys. Chem. B 110, 4318–4322.
Male, K.B., Hrapovic, S., Luong, J.H.T., 2007. Analyst 132, 1254–1261.
Qian, L.H., Chen, M.W., 2007. Appl. Phys. Lett. 91, 083105.
Qiu, H.J., Li, L., Lang, Q.L., Zou, F.X., Huang, X.R., 2012. RSC Adv., doi:10.1039/c2ra01308h, in press.
Qiu, H.J., Lu, L., Huang, X.R., Zhang, Z.H., Qu, Y.B., 2010. Bioresour. Technol. 101, 9415–9420.
Qiu, H.J., Xu, C.X., Huang, X.R., Ding, Y., Qu, Y.B., Gao, P.J., 2008. J. Phys. Chem. C 112, 14781–14785.
Qiu, H.J., Xu, C.X., Huang, X.R., Ding, Y., Qu, Y.B., Gao, P.J., 2009a. J. Phys. Chem. C 113, 2521–2525.
Qiu, H.J., Xue, L.Y., Ji, G.L., Zhou, G.P., Huang, X.R., Qu, Y.B., Gao, P.J., 2009b. Biosens. Bioelectron. 24, 3014–3018.
Scanlon, M.D., Salaj-Kosla, U., Belochapkine, S., MacAodha, D., Leech, D., Ding, Y., Magner, E., 2012. Langmuir 28, 2251–2261.
Shin, T.-Y., Yoo, S.-H., Park, S., 2008. Chem. Mater. 20, 5682–5686.
Shulga, O.V., Jefferson, K., Khan, A.R., D'Souza, V.T., Liu, J., Demchenko, A.V., Stine, K.J., 2007. Chem. Mater. 19, 3902–3911.
Wang, J., Musameh, M., 2003. Anal. Chem. 75, 2075–2079.
Wang, J., Thomas, D.F., Chen, A., 2008. Anal. Chem. 80, 997–1004.
Wittstock, A., Neumann, B., Schaefer, A., Dumuya, K., Kubel, C., Biener, M., Zielasek, V., Steinruck, H., Gottfried, J., Biener, J., Hamza, A., Baumer, M., 2009. J. Phys. Chem. C 113, 5593–5600.
Wittstock, A., Zielasek, V., Biener, J., Friend, C.M., Baumer, M., 2010. Science 327, 319–322.
Xia, Y., Huang, W., Zheng, J.F., Niu, Z.J., Li, Z.L., 2011. Biosens. Bioelectron. 26, 3555–3561.
Xu, C., Su, J., Xu, X., Liu, P., Zhao, H., Tian, F., Ding, Y., 2006. J. Am. Chem. Soc. 129, 42–43.
Yu, F., Ahl, S., Caminade, A.-M., Majoral, J.-P., Knoll, W., Erlebacher, J., 2006. Anal. Chem. 78, 7346–7350.
Zhang, Z., Wang, Y., Qi, Z., Zhang, W., Qin, J., Frenzel, J., 2009a. J. Phys. Chem. C 113, 12629–12636.
Zhang, Z.H., Wang, Y., Qi, Z., Lin, J.K., Bian, X.F., 2009b. J. Phys. Chem. C 113, 1308–1314.
Zhou, M., Zhai, Y.M., Dong, S.J., 2009. Anal. Chem. 81, 5603–5613.
Zielasek, V., Jurgens, B., Schulz, C., Biener, J., Biener, M.M., Hamza, A.V., Baumer, M., 2006. Angew. Chem. Int. Ed. 45, 8241–8244.